J Mater Sci: Mater Electron (2022) 33:3748–3756

Dual-mode optical temperature sensing properties of PIN-PMN-PT:Pr^{3+} ceramic based on fluorescence intensity ratios and lifetimes

Zhen Liu[1,*], Ruixue Wang[1], and Dihu Chen[2,*]

[1] School of Science, Jinling Institute of Technology, Nanjing 211168, China
[2] State Key Laboratory of Optoelectronic Materials and Technologies, School of Electronics and Information Technology, Sun Yat-sen University, Guangzhou 510275, China

Received: 14 October 2021
Accepted: 9 December 2021
Published online: 24 January 2022

ABSTRACT

Pr^{3+} doped PIN-PMN-PT (abbreviated as PIN-PMN-PT:Pr^{3+}) ceramic was successfully fabricated by solid state sintering method. The structural, morphological, and luminescence properties were investigated by X-Ray diffraction, scanning electron microscopy, steady-state photoluminescence, and transient-state photoluminescence spectra. The strong red emission band located at 649 nm can be effectively excited by light centered at 450 nm, 473 nm, and 487 nm, respectively. Under the excitation of light peaking at 487 nm, the temperature-dependent downshifting photoluminescence from 510 nm to 800 nm were recorded in the temperature range of 300 K to 480 K. The obvious luminescence quenching phenomena was detected as the increase of temperature. Based on fluorescence intensity ratio of 620 nm and 649 nm emission bands, the temperature sensing was achieved with maximum relative sensitivity value of 1.73% K^{-1} at 460 K. By studying the temperature-dependent decay curve of transient luminescence, the lifetime of 649 nm emission is confirmed to be sensitive to the change of temperature. Combined the temperature-dependent fluorescence intensity ratio with temperature-dependent fluorescence lifetime, dual-mode temperature sensing was achieved based on photoluminescence. These results show Pr^{3+} doped PIN-PMN-PT ceramic is a promising candidate for thermometry, which may find its applications in the scientific research and industry.

Address correspondence to E-mail: liuzhen@jit.edu.cn; stscdh@mail.sysu.edu.cn

https://doi.org/10.1007/s10854-021-07566-y

1 Introduction

Temperature is a critical physical parameter for both scientific research and industrial application. There are a number of methods that can be used to measure temperature, including liquid expanding, thermocouple, thermistor, and luminescence. Among these methods, thermometry based on photoluminescence has attracted significant attention by virtue of the advantages of non-contact, non-invasive, and fast response, which are suited for applying in some hostile environments such as power station, mines, oil extraction [1–3]. A variety of characteristic spectroscopic parameters are temperature-dependent, including fluorescence intensity, bandshape, spectral shift, lifetime [4]. As a result of these temperature sensitive spectroscopic factors, researchers studied luminescent materials and optical thermometry extensively. Furthermore, numerous cutting-edge works about luminescence thermometry have been reported. Suo et al. investigated the thermally coupled energy levels related fluorescence intensity ratio (FIR) technique for temperature sensing and enhanced the sensitivity by tuning the local symmetry [5]. Xie et al. combined two types of phosphors, each having different emitting centers, into a mixture temperature sensor to enhance the sensitivity of fluorescence intensity ratio technique based on non-thermally coupled energy levels [6]. Liu et al. developed Yb^{3+}, Ho^{3+} doped PMN-PT upconversion multifunctional ceramic and reported the temperature-dependent absolute emission intensity for temperature sensing [7]. Yin et al. reported the position of emission peak of Nd^{3+} doped nanoparticles are temperature sensitive in biological temperature range [8]. Siaï et al. demonstrated the lifetimes of visible emissions for Er^{3+}, Yb^{3+} doped $LaGdO_3$ are temperature-dependent [9]. FIR technology for thermometry is based on two emission bands, which have different temperature-dependent behaviors. It reflects the change in bandshape, is immune to the fluctuations of excitation power, has been studied for a variety of rare earth doped luminescent materials [10–14]. Lifetime for thermometry is based on the temperature relevant kinetic behaviors of emission [15–18]. Due to the fact that the whole spectrum is not required in lifetime based thermometry, it can reduce the effect of heterogeneity of transmittance in medium.

Ferroelectric oxide as host material for rare earth doping has attracted much attentions due to the integrated ferroelectric, piezoelectric, optical properties. Researchers have demonstrated that trace doping rare earth ions in ferroelectric oxides can improve their electric properties [19, 20]. Besides, in recent years, several rare earth doped ferroelectric oxides such as $BaTiO_3$, $(Ba,Ca)(Ti,Zr)O_3$, $K_{0.5}Na_{0.5}NbO_3$, $Bi_{0.5}Na_{0.5}TiO_3$, $Pb(Mg_{1/3}Nb_{2/3})O_3$-$PbTiO_3$, $Pb(In_{1/2}Nb_{1/2})O_3$- $Pb(Mg_{1/3}Nb_{2/3})O_3$-$PbTiO_3$ were utilized for investigating their photoluminescence properties [21–28]. Among above mentioned host materials, $Pb(In_{1/2}Nb_{1/2})O_3$-$Pb(Mg_{1/3}Nb_{2/3})O_3$-$PbTiO_3$ (abbreviated as PIN-PMN-PT) is a kind of ternary relaxor-based ferroelectric solid solution material, which has high curie temperature ($T_c > 180$ °C) and excellent piezoelectric properties ($d_{33} = 2800$ pC/N) [29, 30]. Based on processing optimizing, composition design and doping modification, some modified PIN-PMN-PT based ceramics with excellent electric properties were developed [31–35]. Up to now, there are only a few papers addressing the photoluminescence properties of PIN-PMN-PT ceramics doped with rare earth ions [28, 35]. Thus, it is highly attractive to develop the rare earth doped PIN-PMN-PT luminescent ceramics and study their photoluminescence properties. Pr^{3+} is a desirable rare earth ion for luminescent materials due to its abundant energy levels that can excited by both UV and blue light. And the excitation light source can be achieved by low cost commercial InGaN diode chip [36]. Besides, Pr^{3+} can exhibit strong red emission, which can be used as red component for phosphor-converted white light-emitting diode [37].

In this work, the 26PIN-40PMN-34PT solid solution was chosen as host material. The 26PIN-40PMN-34PT:0.005Pr^{3+} ceramic was synthesized by solid state sintering method. The crystal structure and morphological features were characterized. The photoluminescence excitation spectra was measured and the possible mechanism of photoluminescence was analyzed. The steady-state and transient-state photoluminescence emission spectra of 26PIN-40PMN-34PT:0.005Pr^{3+} ceramic excited by blue light were investigated in detail. Fluorescence intensity ratio and lifetimes analysis were carried out for investigating the temperature sensing properties of the phosphors.

2 Experimental procedures

The Pr^{3+} doped tenary ferroelectric oxide solid solution ceramic was synthesized by columbite precursor solid state sintering method. The 26PIN-40PMN-34PT:0.005Pr^{3+} was selected as the target composition. Firstly, for suppressing the occurrence of sencondary phase, the columbite precursor powders of $InNbO_4$, $MgNb_2O_6$ were prepared via high temperature solid state reaction of stoichiometric high pure In_2O_3, Nb_2O_5 and MgO powders, respectively. Then, the obtained dry precursor powders were mixed with high pure PbO, TiO_2, and Pr_6O_{11} powders followed by grinding with ethanol in agate mortar for 2 h. After grinding, the slurry was dried and the milled dry powders were calcined at 850 °C for 4 h to get the 26PIN-40PMN-34PT:0.005Pr^{3+} powders. After that, the calcined powders were pressed into pellet with diameters of 13 mm. Then, the pellet was sintered at 1250 °C for 6 h to obtain the ceramic.

The crystal structure of as-synthesized ceramic was characterized by X-Ray diffraction (SmartLab, CuKα1 radiation with 0.154 nm, operated at 30 kV, 5 mA) in the 2θ range from 10° to 90°. For the morphological investigation, the scanning electron microscopy was used to observe the grain shape and size of the ceramic. The steady-state photoluminescence excitation spectra and photoluminescence spectra were recorded by spectrometer (Edinburgh Instruments FLS980) equipped with Xenon lamp as light source and PMT optoelectric detector. The temperature dependence of steady-state and transient-state photoluminescence emission spectra were collected at different temperature, which is controlled by a home-made temperature controller. Transient-state photoluminescence decay curves were measured by the spectrometer equipped with a time correlated single photon counter and a pulsed excitation light source. For avoiding the violent disturbance of temperature, the temperature of ceramic sample was hold 3 min before data collection.

3 Results and discussion

For investigating the crystal structure of as-synthesized 26PIN-40PMN-34PT:0.005Pr^{3+} ceramic, the X-Ray diffraction pattern in the range of 10° to 90° is shown in Fig. 1. The position of diffraction peaks can be matched with standard JCPDS Card No.70-0746, indicating the sample possesses pure perovskite phase structure and Pr^{3+} ions are successfully doped into the PIN-PMN-PT host lattice. The inset diagram in Fig. 1 shows the enlarged (002) diffraction peak near 45°. It can be clearly seen that the peak is asymmetrical due to the splitting. The appearing of shoulder peak of (002) near 45° can be attributed to the coexistence of rhombohedral phase and tetragonal phase. The quality of ceramic can be usually evaluated by its microscopic morphology. Figure 2 exhibits the scanning electron microscope image of 26PIN-40PMN-34PT:0.005Pr^{3+} ceramic. The image clearly shows that no obvious pores exist between the grain boundaries, indicating the good quality for ceramic. Moreover, the shapes of grains are irregular and grain sizes are about 2 ~ 5 μm.

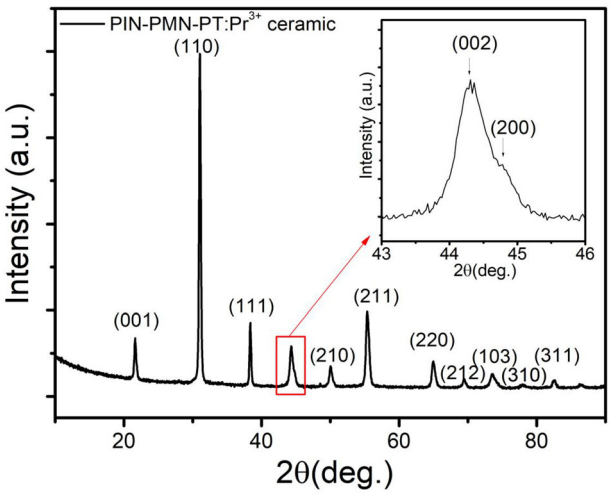

Fig. 1 X-Ray diffraction image of synthesized PIN-PMN-PT:Pr^{3+} ceramic

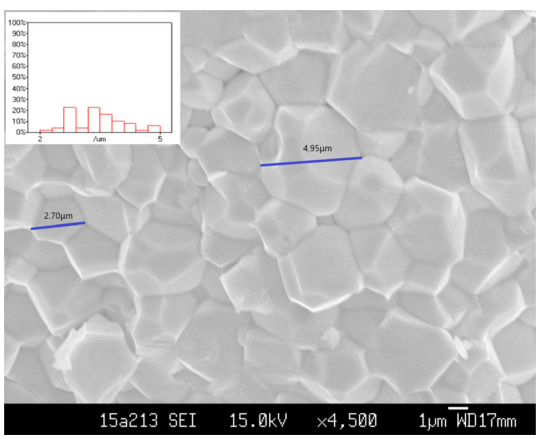

Fig. 2 SEM image of the synthesized PIN-PMN-PT:Pr^{3+} ceramic

For photoluminescence, the selection of excitation wavelength plays vital role in effectively pumping excited state energy levels. Thus, the photoluminescence excitation spectrum monitored at 649 nm emission of **26**PIN-40PMN-34PT:0.005Pr^{3+} ceramic is recorded. Figure 3 displays the photoluminescence excitation spectrum of ceramic sample in spectral range from 400 nm to 500 nm. It is obviously seen that there are three excitation peaks located at 450 nm, 473 nm, 487 nm, which are corresponding to the $^3H_4$-$^3P_2$, $^3H_4$-$^3P_1$, $^3H_4$-$^3P_0$ transitions from ground state to excited state, respectively. Among three main excitation peaks, the spectrum at 487 nm has the strongest intensity, indicating the optimal photoluminescence emission can be obtained upon the 487 nm light excitation. Figure 4 shows the photoluminescence spectrum of ceramic sample excited by 487 nm light at room temperature. It displays seven emission bands centered at 532 nm, 546 nm, 620 nm, 649 nm, 687 nm, 713 nm, 734 nm in the spectral range from 510 nm to 800 nm. By analyzing the emission intensity, we can conclude that red emission band located at 649 nm has the strongest emission intensity. Moreover, the sequence of emission intensity is $I_{649\ nm} > I_{620\ nm} > I_{734\ nm} > I_{713\ nm} > I_{687\ nm} > I_{532nm}$. These downshifting emissions can be explained by transitions from upper excited states to ground state or transitions from upper excited states to lower excited states. Figure 5 shows the schematic energy level diagram of Pr^{3+} ions. As shown in the energy level diagram, the process of photoluminescence in **26**PIN-40PMN-34PT:0.005Pr^{3+} excited by 487 nm light can be explained. Firstly, the Pr^{3+} ions absorb the energy from 487 nm photons, the electrons on ground state energy level are pumped into $^3P_0$ excited state energy level. The electrons on $^3P_0$ energy

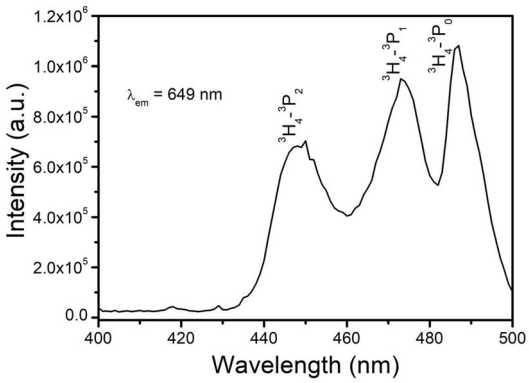

Fig. 3 Photoluminescence excitation spectrum of ceramic sample

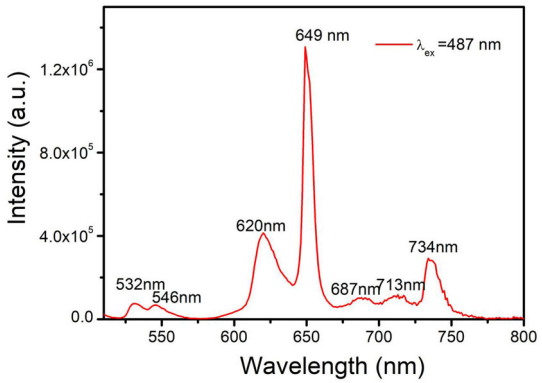

Fig. 4 Photoluminescence spectrum of ceramic sample excited by 487 nm light at room temperature

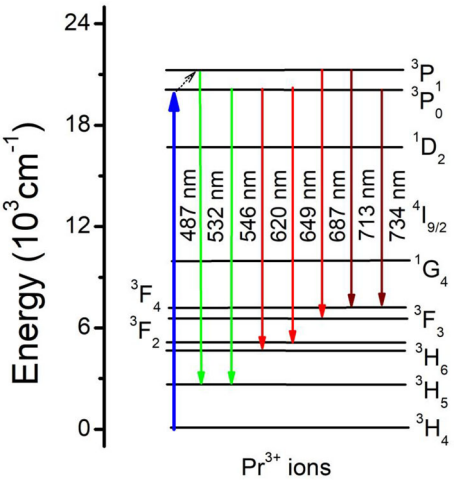

Fig. 5 Schematic energy level diagram of Pr^{3+} ions

level can partly reach the higher energy level $^3P_1$ with assistance of thermal activated phonons. Subsequently, electrons populated on $^3P_{0,1}$ excited state energy levels return to lower energy levels and produce emissions. The dominant red emission around 620 nm and 649 nm can be ascribed to transitions $^3P_0$-$^3H_6$, $^3P_0$-$^3F_2$, respectively. The green emissions located at 532 nm and 546 nm are associated with thermally coupled energy levels related transitions $^3P_{1,0}$-$^3H_5$. The deep red emissions peaked at 681 nm, 731 nm, 734 nm are separately attributed to transitions $^3P_1$-$^3F_3$, $^3P_1$-$^3F_4$, $^3P_0$-$^3F_4$.

For investigating the optical temperature sensing properties of **26**PIN-40PMN-34PT:0.005Pr^{3+} ceramic, the temperature-dependent downshifting photoluminescence spectra are recorded. Figure 6 shows the steady-state downshifting emission in the spectral range from 510 nm to 800 nm upon 487 nm light

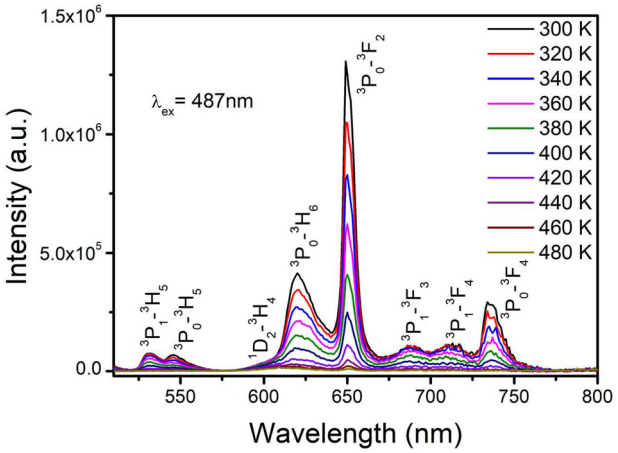

Fig. 6 Temperature-dependent downshifting emission in the spectral range from 510 nm to 800 nm upon 487 nm light excitation

excitation as a function of temperature. The temperature ranges from 300 to 480 K. It is clearly noted that the intensity of emission bands reduce with increase of temperature. This phenomena is due to the luminescence quenching resulted from thermal activation. The integral intensity of dominant emission bands around 620 nm and 649 nm as a function of temperature are shown in Fig. 7. The integral intensity of corresponding emissions decrease with the elevation of temperature, exhibiting strong thermal quenching behaviors. The integral intensity decrease more than 97% for 649 nm emission band and 92% for 620 nm emission band from 300 to 460 K. Usually, the thermal quenching of emission intensity can be describe by the followed Eq. (1).

$$(T) = \frac{I_0}{1 + Ae^{-\frac{\Delta E}{kT}}} \tag{1}$$

where T represents absolute temperature, I(T) is the integral emission intensity at measured temperature T, I_0 is the emission intensity at initial temperature. A, k, and ΔE are constant, Boltzmann constant, activation energy for thermal quenching, respectively.

Considering the different variation trend of emission intensity, 620 nm and 649 nm emission bands are selected for temperature sensing based on fluorescence intensity ratio technology. Figure 8 exhibits the fluorescence intensity ratio between 620 nm and 649 nm emission bands as a function of temperature in the range from 300 K to 460 K. The data of fluorescence intensity ratio versus temperature can be described as the Eq. (2) [38]

$$FIR = B + Ce^{-\frac{D}{T}} \tag{2}$$

B, C, D are fitted parameters associated with above mentioned I_0, A, and ΔE. The solid line in Fig. 8 represents the fitting curve according to Eq. (2). It shows that the data can be well fitted and the fitting curve equation was $FIR = 1.4 \times 10^5 e^{-\frac{5212}{T}} + 0.76$. Uncertainty of FIR is shown by error bar. To evaluate temperature sensing properties based on fluorescence intensity ratio technology, the relative sensitivity can be calculated by the followed formula(3)

$$S_r = \frac{1}{FIR}\left|\frac{dFIR}{dT}\right| \tag{3}$$

Figure 9 displays the sensitivity curve based on the fluorescence intensity ratio method. The sensitivity

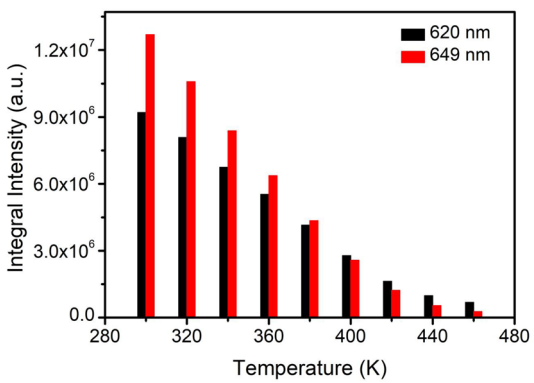

Fig. 7 Integrated intensity of 620 nm and 649 nm emission bands as a function of temperature

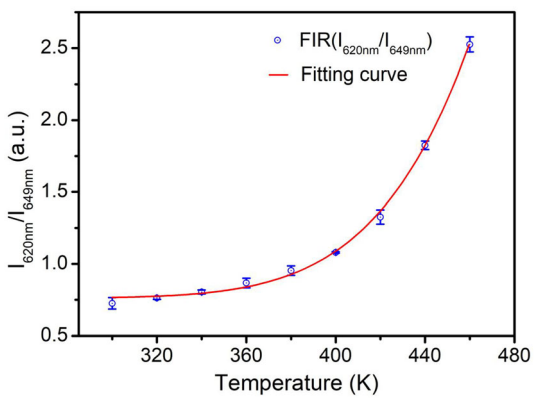

Fig. 8 Fluorescence intensity ratio (I_{620nm}/I_{649nm}) as a function of temperature

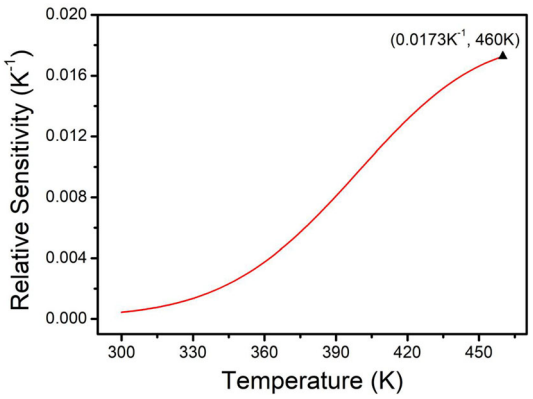

Fig. 9 Relative sensitivity curve of fluorescence intensity ratio thermometry

reaches the 1.73% K^{-1} at 460 K, suggesting the 26PIN-40PMN-34PT:0.005Pr^{3+} ceramic has potential in fluorescence intensity ratio based optical temperature sensing.

To investigate the lifetime based temperature sensing properties of the ceramic sample, decay curves of its dominant emission at 620 nm were measured in the temperature range from 303 K to 463 K. Figure 10 depicts the transient-state photoluminescence spectra at different temperature. The data can be fitted by single exponential function as followed Eq. (4)

$$I(t) = I_0 e^{-\frac{t}{\tau}} + B \tag{4}$$

where $I(t)$ is the emission intensity at t time, I_0 is initial emission intensity after removing the excitation light, τ represents the lifetime, B is fitted constant. It is found the lifetime decreases with temperature enhancement. This phenomena can be explained the multi-phonon relaxation induced by the elevation of temperature. The inversion of lifetime versus temperature is shown in Fig. 11. It can be illustrated by the following formula (5)

$$\frac{1}{\tau} = Ce^{-\frac{\Delta E}{kT}} + \frac{1}{\tau_0} \tag{5}$$

C, k, T are fitted constant, Boltzmann constant, and absolute temperature, respectively. ΔE is activation energy related to thermal quenching process. τ_0 represents lifetime of emission when temperature is zero. The fitting results show the formula can be expressed as $\frac{1}{\tau} = 1.05 \times e^{-\frac{3775.36}{T}} + 1.25 \times 10^{-4} \mathrm{ns}^{-1}$. Error bars are utilized to describe the luminescence lifetime uncertainty.

For evaluating performance of the lifetime based temperature sensing, temperature-dependent relative sensitivity is calculated by Eq. (6)

$$S_r = \left| \frac{d(1/\tau)}{(1/\tau)dT} \right| \tag{6}$$

The sensitivity curve of lifetime based thermometry is shown in Fig. 12. It can be found the relative sensitivity increases monotonously with temperature enhancement and reaches its maximum value at 463 K. It suggests that lifetime thermometry based on photoluminescence of 26PIN-40PMN-34PT:0.005Pr^{3+} ceramic upon 487 nm light excitation is possible. Thus, dual-mode temperature sensing can be achieved by combining with fluorescence intensity ratio thermometry.

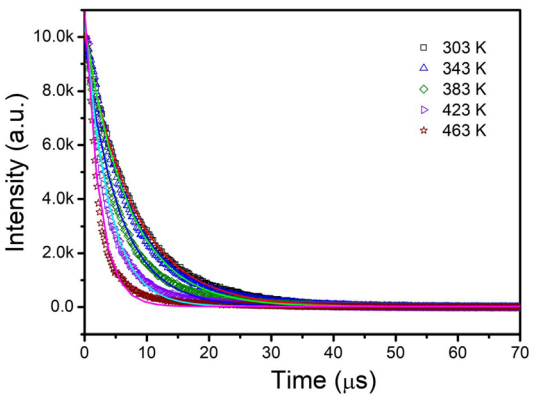

Fig. 10 Transient-state photoluminescence spectra at different temperature

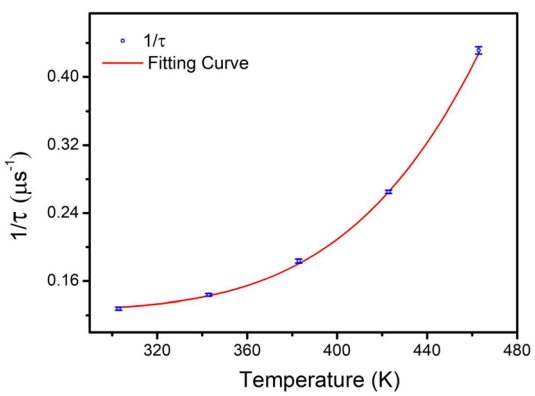

Fig. 11 The inversion of lifetime as a function of temperature

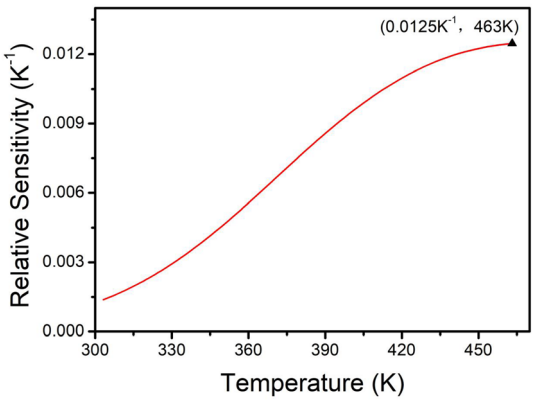

Fig. 12 Relative sensitivity curve of lifetime thermometry

4 Conclusion

26PIN-40PMN-34PT:0.005Pr^{3+} ceramic was synthesized by solid state sintering method. The down-shifting photoluminescence was investigated. The investigation of temperature sensing properties based on both steady-state and transient-state photoluminescence have been carried out. For steady-state photoluminescence, the fluorescence intensity ratio thermometry based on 620 nm and 649 nm emission bands of sample upon 487 nm excitation was successfully achieved. The maximum relative sensitivity is 1.73% K^{-1}. For transient-state photoluminescence, the lifetime thermometry based on decay properties of 649 nm emission was proved. It has the maximum relative sensitivity of 1.25% K^{-1}. Results shown in this work suggest that 26PIN-40PMN-34PT:0.005Pr^{3+} ceramic has great potential in dual-mode temperature sensing.

Acknowledgements

This work is financially supported by the Research Start-up Program of Jinling Institute of Technology (jit-b-202054), the National Natural Science Foundation of China (Grant Nos. 81471787 and 61471401).

Author contribution

ZL: Data curation, Writing, Resources. RW: Review & Editing. DC: Supervision, Review, Resources.

Data availability

The datasets generated during and/or analyzed during the current study are available from the corresponding author on reasonable request.

Declarations

Conflict of interest The authors declare that they have no known competing financial interests or personal relationships that could have appeared to influence the work reported in this paper.

References

1. Y. Huang, A. Skripka, L. Labrador-Páez, F. Sanz-Rodríguez, P. Haro-González, D. Jaque, F. Rosei, F. Vetrone, Upconverting nanocomposites with combined photothermal and photodynamic effects. Nanoscale **10**, 791–799 (2018)
2. Z. Liang, F. Qin, Y.D. Zheng, Z.G. Zhang, W.W. Cao, Sens. Actuators A Phys. **238**, 215–219 (2016)
3. H. Li, Y.D. Zhang, L. Shao, Z.M. Htwe, P. Yuan, Luminescence probe for temperature sensor based on fluorescence intensity ratio. Opt. Mater. Express **7**, 1077–1083 (2017)
4. C.D.S. Brites, S. Balabhadra, L.D. Carlos, Lanthanide-based thermometers: At the cutting-edge of luminescence thermometry. Adv. Opt. Mater. **7**, 1801239 (2019)
5. H. Suo, X.Q. Zhao, Z.Y. Zhang, R. Shi, Y.F. Wu, J.M. Xiang, C.F. Guo, Local symmetric distortion boosted photon upconversion and thermometric sensitivity in lanthanum oxide Nanospheres. Nanoscale **10**, 9245–9251 (2018)
6. C.Y. Xie, P. Wang, Y. Lin, X.T. Wei, Y.H. Chen, M. Yin, Temperature dependent lumnescence of a phosphor mixture of $Li_2TiO_3:Mn^{4+}$ and $Y_2O_3:Dy^{3+}$ for dual mode optical thermometry. J. Alloy. Compd. **821**, 152467 (2020)
7. Z. Liu, G.C. Jiang, R.X. Wang, C.K. Chai, L.M. Zheng, Z.G. Zhang, B. Yang, W.W. Cao, Temperature and concentration effects on upconversion photoluminescence properties of Ho3+ and Yb3+ codoped 0.67Pb(Mg1/3Nb2/3)O3–0.33PbTiO3 multifunctional ceramics. Ceram. Int. **42**, 11309–11313 (2016)
8. G.C. Jiang, X.T. Wei, S.S. Zhou, Y.H. Chen, C.K. Duan, M. Yin, Neodymium doped lanthanum oxysulfide as optical temperature sensors Author links open overlay panel. J. Lumi. **152**, 156–159 (2014)
9. A. Siaï , P. Haro-Gonzalez, K. Horchani Naifer, M. Ferid, Optical temperature sensing of Er^{3+}/Yb^{3+} doped $LaGdO_3$ based on fluorescence intensity ratio and lifetime thermometry, Opt. Mater. **76**, 34–41 (2018)

10. H.L. Zhou , N.An , K. S. Zhu, J. R. Qiu, L. H. Yue, L. G. Wang , L. H. Ye , Optical temperature sensing properties of Tm^{3+}/Yb^{3+} co-doped LuAG polycrystalline phosphor based on up-conversion luminescence, J. Lumi. **229**, 117656 (2021)
11. K. Pavani, J.P.C. do Nascimento, S.K. Jakka, F.F. do Carmo, A.J.M. Sales, M. J. Soares, M.P.F. Graça, F.J.A. de Aquino, D.X. Gouveia, A.S.B. Sombra, Analogy of different optical temperature sensing techniques in $LaNbO4:Er^{3+}/Yb^{3+}$ phosphor, J. Lumi. **235**, 117992 (2021)
12. M. Sójka, J. F. C. B. Ramalho, C. D. S. Brites, K. Fiaczyk, L. D. Carlos, E. Zych, Bandgap engineering and excitation energy alteration to manage luminescence thermometer performance. The case of $Sr_2(Ge,Si)O_4:Pr^{3+}$, Adv. Opt. Mater. **7**, 1901102 (2019)
13. A.M. Kaczmarek, M.K. Kaczmarek, R.V. Deun, Er^{3+}-to-Yb^{3+} and Pr^{3+}-to-Yb^{3+} energy transfer for highly efficient near-infrared cryogenic optical temperature sensing. Nanoscale **11**, 833–837 (2019)
14. F.J. Caixeta, A.R.N. Bastos, A.M.P. Botas, L.S. Rosa, V.S. Souza, F.H. Borges, A.N.C. Neto, A. Ferrier, P. Goldner, L.D. Carlos, R.R. Gonçalves, R.A.S. Ferreira, High-quantum-yield upconverting Er^{3+}/Yb^{3+}-organic–inorganic hybrid dual coatings for real-time temperature sensing and photothermal conversion. J. Phys. Chem. C **124**, 19892–19903 (2020)
15. O.A. Savchuk, P. Haro-Gonzalez, J.J. Carvajal, D. Jaque, J. Massons, M. Aguilo, F. Diaz, $Er:Yb:NaY_2F_5O$ up-converting nanoparticles for sub-tissue fluorescence lifetime thermal sensing. Nanoscale **6**, 9727–9733 (2014)
16. A. Siai, P. Haro-Gonzalez, K. Horchani-Naifer, M. Ferid, La_2O_3:Tm, Yb, Er upconverting nano-oxides for sub-tissue lifetime thermal sensing. Sens. Actuators B Chem. **234**, 541–548 (2016)
17. S. Gharouel, L. Labrador-Páez, P. Haro-González, K. Horchani-Naifer, M. Férid, Fluorescence intensity ratio and lifetime thermometry of praseodymium phosphates for temperature sensing. J. Lumi. **201**, 372–383 (2018)
18. L. Yao, D.K. Xu, Y.J. Li, H. Lin, S.H. Yang, Y.L. Zhang, Regulation of morphologies and luminescence of β-$NaGdF_4:Yb^{3+}$, $E^{r3}+$ upconversion nanoparticles by hydrothermal method and their dual-mode thermometric properties. Appl. Surf. Sci. **466**, 320–327 (2019)
19. F. Li, M.J. Cabral, B. Xu, Z.X. Cheng, E.C. Dickey, J.M. LeBeau, J.L. Wang, J. Luo, S. Taylor, W. Hackenberger, L. Bellaiche, Z. Xu, L.Q. Chen, T.R. Shrout, S.J. Zhang, Giant piezoelectricity of Sm-doped $Pb(Mg_{1/3}Nb_{2/3})O_3$-$PbTiO_3$single crystals. Science **364**, 264–268 (2019)
20. S.S. Dong, F.F. Guo, H.Q. Zhou, W. Long, P.Y. Fang, X.J. Li, Z.Z. Xi, Phase structures and electrical properties of Sm doped PSN-PMN-PT ceramics. J. Alloy. Compd. **881**, 160621 (2021)
21. Z. Wu, Y. Zhang, G. Bai, W. Tang, J. Gao, J. Hao, Effect of biaxial strain induced by piezoelectric PMN-PT on the upconversion photoluminescence of BaTiO3:Yb/Er thin films. Opt. Express **22**, 29014–29019 (2014)
22. H.S. Chen, Z.G. Dong, Y.N. Zhao, S.S. Li, X.N. Du, Z.P. Wu, W.W. Liu, Y. Zhang, In-situ tailoring upconversion processes from lanthanide ions doped ferroelectric films through piezoelectric strain. J. Lumi. **219**, 116914 (2020)
23. J. Xu, Y. Zhou, Z.H. Li, C. Lin, X.H. Zheng, T.F. Lin, X. Wu, F.F. Wang, MIcrostructural, ferroelectric and photoluminescence properties od Er3+ doped $Ba_{0.85}Ca_{0.15}Ti_{0.9}Zr_{0.1}O_3$ thin films. Mater. Chem. Phys. **262**, 124320 (2021)
24. C. Lin, H.J. Wang, P. Wang, X. Wu, T.F. Lin, B.S. Sa, Y. Cheng, X.H. Zheng, X. Yu, C.Q. Fang, Smart white lighting and multi-mode optical modulations via photochromism in Dy-doped KNN-based transparent ceramics. J. Am. Ceram. Soc. **104**, 903–916 (2021)
25. H.Q. Sun, Q.W. Zhang, X.S. Wang, Y. Zhang, The photoluminescence and electrical properties of lead-free (Bi0.5Na0.5)TiO3: Pr ceramics. Ceram. Int. **40**, 15669–15675 (2014)
26. H.Q. Sun, Q.W. Zhang, X.S. Wang, T. Zhang, $Bi_{0.5}Na_{0.5}$-$TiO_3:Eu^{3+}$: an intense blue converting red phosphor. Mater. Lett. **131**, 164–166 (2014)
27. Z. L. Lv, Y. L. Qin, Y. C. Zhang, J. J. Fu, C. J. Lu, Efficient upconversion photoluminescence in transparent Pr^{3+}/Yb^{3+} co-doped $0.75Pb(Mg_{1/3}Nb_{2/3})O_3$–$0.25PbTiO_3$ ferroelectric ceramics, Ceram. Int. **45**, 10924–10929 (2019)
28. Z. Liu, D. H. Chen, Upconversion photoluminescence and dual mode temperature sensing properties of PIN-PMN-$PT:Er^{3+}$ ceramic, J. Alloy. Compd. **815**, 152092 (2020)
29. Z.H. Li, Y.C. Wang, Y.X. Tang, X.Y. Zhao, T. Wang, Z.H. Duan, F.F. Wang, X.B. Li, C.M. Leung, B.J. Fang, Growth and electrical properties of high-Curie point rhombohedral $Mn\text{-}Pb(In_{1/2}Nb_{1/2})O_3\text{-}Pb(Mg_{1/3}Nb_{2/3})O_3\text{-}PbTiO_3$ thin films. J. Am. Ceram. Soc. **104**, 313–321 (2021)
30. J.W. Chen, X.B. Li, X.Y. Zhao, X.A. Wang, C. Chen, H. Deng, B. Ren, J. Jiao, H.S. Luo, Compositional segregation, structural transformation and property-temperature relationship of high-curie temperature $Pb(In_{1/2}Nb_{1/2})O_3$-$Pb(Mg_{1/3}Nb_{2/3})O_3$-$PbTiO_3$ single crystals. J. Mater. Sci-Mater Electr. **26**, 9316–9328 (2015)
31. B.H. Watson III., M.J. Brova, Y.F. Chang, S.T. Misture, M.A. Fanton, R.J. Meyer Jr., G.L. Messing, Low temperature reactive sintering of CuO-doped PIN-PMN-PT ceramics. J. Eur. Ceram. Soc. **39**, 4719–4726 (2019)
32. B.H. Watson III., M.J. Brova, M.A. Fanton, R.J. Meyer Jr., G.L. Messing, Densification and properties of oxygen sintered CuO-doped PIN-PMN-PT ceramics. J. Eur. Ceram. Soc. **40**, 3956–3964 (2020)

33. B.H. Watson III., M.J. Brova, M.A. Fanton, R.J. Meyer Jr., G.L. Messing, Textured Mn-doped PIN-PMN-PT ceramics: harnessing intrinsic piezoelectricity for high-power transducer applications. J. Eur. Ceram. Soc. **41**, 1270–1279 (2021)
34. J. Wu, Y.F. Chang, B. Yang, X.H. Wang, S.T. Zhang, Y. Sun, X.D. Qi, J.J. Wang, W.W. Cao, Densification behavior and electrical properties of CuO-doped $Pb(In_{1/2}Nb_{1/2})O_3$-$Pb(Mg_{1/3}Nb_{2/3})O_3$-$PbTiO_3$ ternary ceramics. Ceram. Int. **42**, 7223–7229 (2016)
35. X.D. Qi, Y. Zhao, E.W. Sun, J. Du, K. Li, Y. Sun, B. Yang, R. Zhang, W.W. Cao, Large electrostrictive effect and high energy storage performance of Pr^{3+}-doped PIN-PMN-PT multifunctional ceramics in the ergodic relaxor phase. J. Eur. Ceram. Soc. **39**, 4060–4069 (2019)
36. T.R. Raman, Y.C. Ratnakaram, B.D.P. Raju, Synthesis and spectroscopic investigations on Pr^{3+}-doped $LiPbB_5O_9$ phosphor: a blue converting red phosphor for white LEDs. Optik **225**, 165758 (2021)
37. B. Han, Y.Z. Dai, J. Zhang, X.Y. Wang, W.H. Shi, H.Z. Shi, $NaLaMgWO_6$:Pr^{3+}: a novel blue- light excitable red-emitting phosphor for white light-emitting diodes. J. Lumin. **196**, 275–280 (2018)
38. Q. Wang, M. Liao, Q.M. Lin, M.X. Xiong, Z.F. Mu, F.G. Wu, A review on fluorescence intensity ratio thermometer based on rare earth and transition metal ions doped inorganic luminescent materials. J. Alloy. Compd. **850**, 156744 (2021)